NUMERICAL SIMULATION OF GAS–DROPLET FLOW AROUND A NOZZLE IN A CYLINDRICAL CHAMBER USING A LAGRANGIAN MODEL BASED ON A MULTIGRID NAVIER–STOKES SOLVER

Th. Frank , I. Schulze
Technical University of Chemnitz–Zwickau
Department of Mechanical Engineering III
Research Group of Multiphase Flow
Chemnitz, Germany

1. ABSTRACT

A numerical simulation of an upward directed, 2–dimensional, turbulent gas–droplet flow around an axisymmetric nozzle in a cylindrical chamber was made. We use a Lagrangian method, where trajectories of many droplets are calculated from the equations of motion along with the continuity and momentum equations of fluid. Strong coupling effects between the two phases are dealt with. Special algorithms were introduced for particle tracking and interpolation of the fluid flow data at the particle location on the numerical grid, which use multigrid structure for improvement of the speed of droplet trajectory calculation. The Lagrangian solver for the calculation of the trajectory and particle momentum source term was parallelised on a workstation cluster using a host–node programming model. The resulting droplet and fluid velocities at different cross sections of the cylindrical chamber are reported and compared with measurements.

2. INTRODUCTION

In many engineering flow situations particulate two–phase flows play an important role. The motion of particles or droplets in a turbulent flow has been studied theoretically, numerically and experimentally for more than 40 years. In the last decade the modelling of two–phase flows has been performed in several different ways. The continuous phase is usually predicted from an Eulerian approach and the behaviour of discrete particles is predicted from either an Eulerian or a Lagrangian approach. The performances of each approach have been studied in detail in the literature by e.g. Durst et al. [3] and Crowe [2].

The objective of this work was to develop, test and validate a numerical algorithm for the prediction of particulate two–phase flows in particular for flow regimes in gas cleaning and spray drying facilities. An Eulerian/Lagrangian stochastic–deterministic (LSD–)model was incorporated in the FASTEST (**F**low **A**nalysis by **S**olving **T**ransport **E**quations with **S**imulated **T**urbulence) code developed by M. Perić and A.D. Gosman. The Lagrangian particle trajectory solver was specially adapted to the non–orthogonal, boundary–fitted arbitrary numerical grids used by the Navier–Stokes solver and to the full multigrid solution scheme implemented in FASTEST. The PSI–cell model developed by Crowe et al. [1] has been used. The chosen test flow case was a cylindrical, vertical upward directed, turbulent gas–droplet flow. It is perturbed by a 90° jet from a solid cone nozzle located on the axis of symmetry. This jet can be directed either in upward or downward direction. The flow is assumed to be axisymmetric and corresponds to the experiments of Schulze et al.'s [12, 13].

3. EQUATIONS OF FLUID MOTION

3.1. The Coordinate system

The coordinate system is shown in Fig. 1. The fluid motion is determined on a cylindrical grid (x, r) benefitting from the radial symmetry of the problem. The
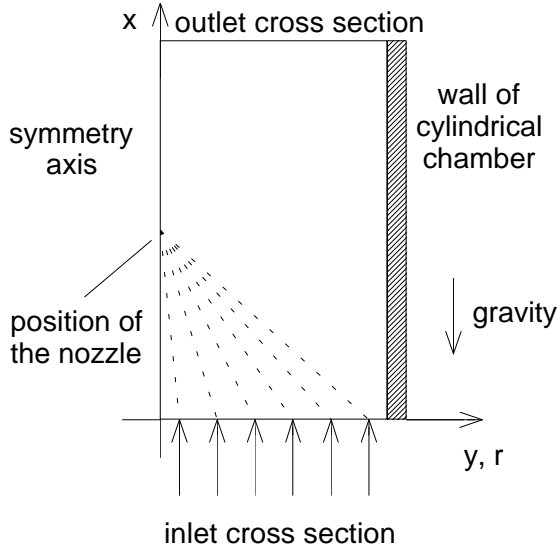
Figure 1: Geometry and coordinate system.

x–axis is in the direction of the vertical main stream, the r–axis is in the horizontal direction. For the calculation of the droplet motion, the Cartesian coordinate system (x, y) is adopted.

3.2. Fundamental equations

The turbulent two–phase (gas–droplet) flow under consideration is described by assuming that the particulate phase is dilute, but the particle loading is appreciable. Inter–particle effects are neglected, but the effects of the particles on the gas flow are taken into account. The two–phase flow is statistically stationary, incompressible and isothermal. The gas phase has constant physical properties and is Newtonian. Under these assumptions the time–averaged form of the governing gas–phase equations can be cast into the following form of the general transport equation :

$$
\frac{\partial}{\partial x}(\rho_F\, u_F\, \Phi) \;+\; \frac{1}{r}\frac{\partial}{\partial r}(r\,\rho_F\, v_F \Phi) = \frac{\partial}{\partial x}\left(\Gamma\,\frac{\partial \Phi}{\partial x}\right)
$$
$$
+\; \frac{1}{r}\frac{\partial}{\partial r}\left(r\,\Gamma\,\frac{\partial \Phi}{\partial r}\right) + S_\Phi + S_\Phi^P \quad (1)
$$

where Φ stands for u_F, v_F, k and ε. The terms S_Φ and Γ represent the "source" and the effective diffusion coefficient, respectively, and S_Φ^P represents the coupling through the particle–fluid interaction. This last term is calculated by solving the Lagrangian equation of particle motion. The continuity equation is obtained by setting $\Phi = 1$, $\Gamma = 0$.

For modelling of fluid turbulence the standard k–ε turbulence model together with isotropic eddy viscosity and standard model constants are used :

$$
\mu_t \;=\; C_\mu\,\rho_F\,\frac{k^2}{\varepsilon} \quad , \quad \Gamma_\Phi^t = \frac{\mu_t}{\sigma_\Phi}
$$
$$
S_k \;=\; P_k - \rho_F\,\varepsilon
$$
$$
S_\varepsilon \;=\; C_{\varepsilon_1}\frac{\varepsilon}{k}\,P_k - C_{\varepsilon_2}\,\rho_F\,\frac{\varepsilon^2}{k} \quad (2)
$$

$$
C_\mu = 0.09 \quad , \quad C_{\varepsilon_1} \;=\; 1.44 \quad , \quad C_{\varepsilon_2} = 1.92
$$
$$
\sigma_k = 1.0 \quad , \quad \sigma_\varepsilon = 1.33
$$

where P_k is the rate of production of turbulence. The influence of particle motion on fluid turbulence characteristics was neglected $(S_k^P = S_\varepsilon^P = 0)$.
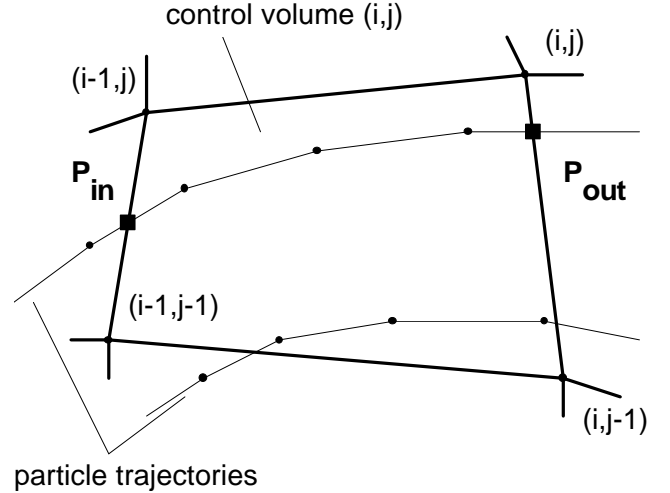

Figure 2: The PSI-cell model. Calculation of particle momentum source terms.

3.3. Particle momentum source term

In the PSI-cell model [1, 2], the force excerted on a fluid control volume by a single particle is calculated from the residence time of a particle in the control volume and the change in particle momentum in that time. In order to calculate the particle momentum source terms $S_{u_F}^P$ and $S_{v_F}^P$ in the momentum equations the points of intersection of the particle trajectory with the faces of the control volume have to be calculated and the particle and fluid properties have to be interpolated in this points (Fig. 2). The particle momentum source term is then as follows :

$$S^P_{u_{F_i}} = \sum \dot{N}_P \, \rho_F \, \frac{A_P}{2} \int_{t_{in}}^{t_{out}} C_D \, v_{rel} \left(u_{Fi} - u_{Pi} \right) dt \quad (3)$$

where the summation is taken over all the representative particles crossing the control volume. Because the number of test particles used for simulation is limited and different from that of particles which would actually cross the control volume, $\dot{N}_P$ characterises the particle flow rate for a calculated representative particle trajectory.

3.4. Solution procedure

The above equations of fluid motion were solved with the FASTEST program package developed by Perić and Gosman [9]. The code is designed for prediction of two-dimensional (plane or axisymmetric), laminar or turbulent, incompressible flows of Newtonian fluid in domains of arbitrary geometry. The numerical solution method employed in the code is based on the finite volume discretization of the governing equations. Characteristics of the method are : use of non–orthogonal, boundary fitted arbitrary numerical grids; colocated arrangement of variables on numerical grids; use of Cartesian vector and tensor components; segregated solution approach of SIMPLE kind [7]; full multigrid solving methodology using local bisectional grid refinement strategy [8].

The original computer code was extended by introduction of the particle momentum source terms in the momentum equations of fluid motion. Efficiency of the solution method was ensured by employing an optimized underrelaxation practice concerning not only the fluid variables but also the additional source terms.

4. EQUATIONS OF DROPLET MOTION IN FLUID

4.1. Equations of motion of the dispersed phase

The droplet phase was treated by the Lagrangian approach where a large number of droplets were followed in time along their trajectories through the flow domain. Each droplet trajectory is assoziated with a droplet flow rate $\dot{N}_P$ and so represents a number of real droplets with the same physical properties. This representation is used in order to allow the consideration of the droplet size distribution and to simulate the appropriate liquid mass flow rate at the injection locations. The droplet trajectories were determined by solving the ordinary differential equations for the droplet location

and velocity components. For the formulation of the droplets equation of motion it was assumed that forces due to droplet rotation, the pressure gradient in the flow, the added mass force and the Basset history force are negligible since a large density ratio ρ_P/ρ_F is considered. The equations of droplet motion than can be written as follows :

$$\frac{d\,x_P}{dt} \;=\; u_P \quad , \quad \frac{d\,y_P}{dt} = v_P$$

$$\frac{d}{dt}\left[\begin{array}{c} u_P \\ v_P \end{array}\right] \;=\; \frac{3}{4}\frac{\nu\,\rho_F}{\rho_P\,d_P^2}Re_P\,C_D(Re_P)\left[\begin{array}{c} u_F - u_P \\ v_F - v_P \end{array}\right]$$

$$+\;\frac{\rho_P - \rho_F}{\rho_P}\left[\begin{array}{c} -g \\ 0 \end{array}\right] \qquad (4)$$

with :

$$Re_P \;=\; \frac{d_P\,v_{rel}}{\nu} \qquad (5)$$

$$v_{rel} \;=\; \sqrt{(u_F - u_P)^2 + (v_F - v_P)^2} \qquad (6)$$

where d_P – droplet diameter; u_P, v_P – droplet velocity components in Cartesian coordinate system (x, y); C_D – coefficient of drag; g – gravity acceleration; ν – fluid kinematic viscosity; ρ – density of the fluid (F) and the droplets (P) respectivly. The drag coefficient C_D is calculated as a function of Re_P using the correlations obtained by Morsi and Alexander [5].

The boundary conditions for the droplet tracking procedure are specified as follows. Trajectories are calculated until the droplet leaves the flow domain through a inlet or outlet cross section. Droplets leaving the computational domain at the symmetry line ($y = 0$) are replaced by droplets entering the domain with opposit radial velocity. For the droplet–wall interaction simple reflection with a restitution coefficient of 0.5 is assumed presently.

4.2. Lagrangian–stochastic–deterministic (LSD) turbulence model

The effect of turbulence of the gas flow on the droplet motion was modelled by a stochastic procedure, the so–called LSD turbulence model proposed by Schönung [10], Schuh et al. [11] and Milojević [4]. The mean fluid velocities u_F, v_F in the above equations of droplet motion (4) are replaced by the instantaneous fluid velocities U_F, V_F which are calculated as the sum of mean

local gas velocities and fluctuation velocities. The values of the fluctuation velocities u'_F and v'_F are sampled from a Gaussian distribution function which is characterized by 0 statistical mean and a standard deviation σ determined from the fluid r.m.s. value which is evaluated from the turbulent kinetic energy by assuming isotropic turbulence.

$$U_F = u_F + u'_F \quad , \quad V_F = v_F + v'_F \quad , \quad \sigma = \sqrt{\frac{2}{3}k} \quad (7)$$

Further is assumed that the droplet motion is influenced by this fluctuation velocities for a certain time period, the interaction time. During this interaction time droplet motion is controlled by the equations of droplet motion (4). The interaction time with one fluid eddy is limited by the eddy life time or the transit time needed for the droplet to traverse the eddy. According to the procedure of Ormancey et al. [6], the eddy death probability during one time step of the Lagrangian solving algorithm is calculated as the ratio of time step size and the Lagrangian time scale. New fluctuation velocities u'_F, v'_F are sampled when a uniformly distributed random number $\alpha \in [0, 1]$ becomes smaller than the eddy death probability :

$$\alpha < \frac{\Delta t}{T_L} \quad , \quad T_L = 0.3\frac{k}{\varepsilon} \quad (8)$$

The crossing trajectory effect is accounted for by integrating the particle travel distance within one eddy and comparing it with the eddy length scale L_E :

$$x_E^n \quad > \quad L_E \quad (9)$$

$$L_E = 0.245\frac{k^{3/2}}{\varepsilon} \quad , \quad x_E^n = x_E^{n-1} + \Delta t \, v_{rel}$$

New fluctuation velocities u'_F, v'_F are sampled when the travel distance x_E^n becomes greater than the eddy length scale, which means that the droplet enters a new eddy.

4.3. Solution procedure and adaptation to the multigrid Navier–Stokes solver

The equations of motion were solved using a standard Runge–Kutta solution scheme of 4th order accuracy with automatic time step correction. In order to ensure sufficient resolution of the influence of fluid flow turbulence on the droplet motion the time step Δt was limited to a maximum of $1/10$ the Lagrangian time scale T_L of the generated eddy.

The numerical procedure to obtain a converged solution for both phases is as follows :

1. A converged solution of the gas flow field was calculated without source terms of the dispersed phase.

2. A large number of droplets were traced through the flow field, and the values of the source terms were calculated for all control volumes of the numerical grid.

3. The flow field was recalculated by considering the source terms of the dispersed phase, where appropriate underrelaxation factors were considered.

4. Repetition of steps 2 and 3 until convergence was reached.

In order to perform the calculation of droplet trajectories in the flow domain in the way described above, it is necessary to have procedures that determine the initial and current position of the droplet on the numerical grid and procedures that interpolate fluid properties like u_F, v_F, k and ε at the current droplet position. On simple orthogonal, rectangular grids often used for channel or pipe flow calculations the droplet localization problem can easy be solved by comparison of the droplet coordinates (x_P, y_P) with the coordinates of the control volume faces which are parallel to the axes of the coordinate system :

$$x_{i-1} \leq x_P \leq x_i \quad , \quad y_{i-1} \leq y_P \leq y_i \quad (10)$$

In the case of non–orthogonal, boundary–fitted arbitrary numerical grids used by e.g. the Navier–Stokes solver FASTEST the droplet localization problem becomes a more computational time consuming task because the (i, j) numbering of control volumes is no longer associated by simple analytical or tabular expressions with the coordinates of control volume faces or corners. In the worst case each control volume of the numerical grid has to be checked for droplet location at the beginning of the trajectory calculation process and at every time step of the Runge–Kutta solving method what results in a sharp increase in computational time of the Lagrangian solver.

In the algorithm presented here the speed of droplet trajectory calculations was improved using the multigrid structure of the numerical grid incorporated

grid level k → grid level k+1

$(i,j)_k$

$(i,j)_{k+1}$

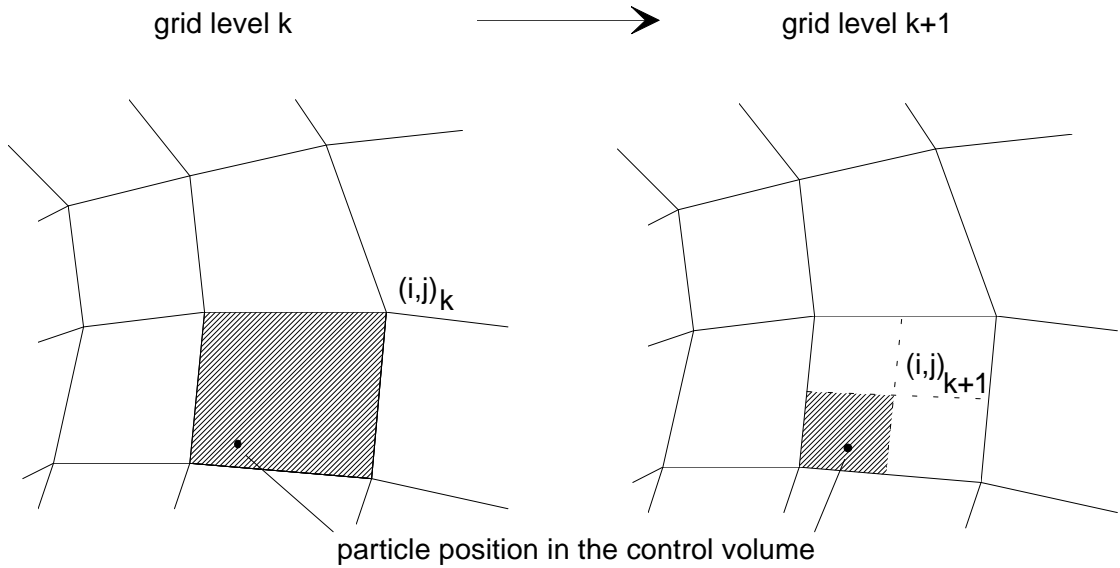particle position in the control volume

Figure 3: "Zoom" on the next finer grid level in search for the droplet location on the numerical grid.

in FASTEST and the bisectional refinement strategy, where a control volume on a coarser grid is divided in 4 control volumes on the next finer grid. The number of grid levels is not limited by the algorithm. So the search for the initial droplet location is performed over all control volumes only on the coarsest grid (first grid level) until the control volume, the droplet trajectory starts in, is found. Once the droplet location on the coarsest grid was found, a "zoom" onto the highest grid level is executed (Fig. 3). Only at most 4 control volumes have to be checked for droplet location at each step of the "zoom" process.

If the droplet location on the numerical grid at the moment t is known the droplet location at the moment $t + \Delta t$ (after a Runge–Kutta time step) is determined by projection of the old droplet location $(i_k, j_k)|_t$ onto the coarsest grid and by performing a "circular search" shown in Fig. 4 around the control volume of the old droplet location $(i_1, j_1)|_t$. If the new droplet location on the coarsest grid $(i_1, j_1)|_{t+\Delta t}$ could be found, a "zoom" on the finest grid is executed again.

Interpolation of u_F, v_F, k and ε at the droplet position is than performed with the values of fluid properties stored at the corner locations of the control volume of the finest grid $(i_k, j_k)|_t$.

4.4. Parallelisation of droplet trajectory calculations

Further improvement of the computational speed of droplet trajectory calculations was achieved through parallelization of the Lagrangian solver. The target system for the parallelized program was a network of HP 735/755 workstations with large amount of local memory. The parallelization was based on the EXPRESS library of communication routines.

The implementation corresponds to the host–node programming model (see Fig. 5). The host program reads first the numerical grid and fluid flow data and distributes them to all node programs. After the generation of initial conditions for the droplet trajectories the host program waits for requests from node programs. On demand the host sends the initial conditions for one trajectory to the node sending the request. Node programs are calculating the droplet trajectories and the corresponding momentum source terms simultanously. After calculation of all droplet trajectories the host program calculates the global sum of all momentum source terms over all nodes and control volumes. Automatic load balancing is achieved by distribution of initial conditions for trajetories on demand. The small amount of communication between host and node programs results in a approximatly ideal speedup of the trajectory calculation process.
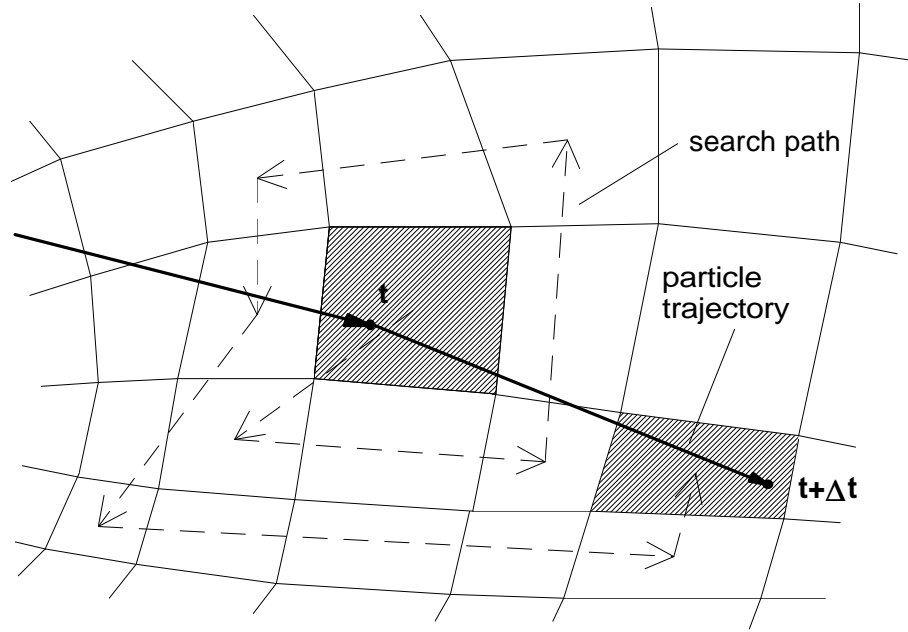
Figure 4: "Circular search" around the control volume of the old droplet location.

In a further step of program development the Navier–Stokes solver has to be parallelized too. The Lagrangian solver has to be modified to run on distributed grid and fluid flow data. With this modifications the program will be able to run not only on workstation clusters but also on dedicated parallel computer architectures (e.g. MIMD computers) with a great number of computational nodes and smaller amounts of local memory.

5. RESULTS AND DISCUSSION

5.1. Flow configuration and conditions of simulation

For the chosen test case flow configuration corresponds to Schulze et al.'s [12, 13] experiments. Gas flow at normal temperature enters a vertical cylindrical test section with a uniform velocity distribution at the inlet cross section (Fig. 1). The geometry data and physical properties of air flow have the following values :

Radius of test section	R	$= 1.5\,m$
Height of test section	H	$= 6.0\,m$
Air density	ρ_F	$= 1.0786\,kg/m^3$
Kinematic viscosity	ν_F	$= 1.821 \cdot 10^{-5}\,m^2/s$

A solid cone nozzle with downward directed jet was mounted on the symmetry axis of the test section at $x = 2.75\,m$. The characteristics of the nozzle and the jet of droplets are :

Diameter of the nozzle	D_N	$= 0.1\,m$
Initial cone angle of the nozzle	α_N	$= 90°$
Droplet density	ρ_P	$= 994\,kg/m^3$
Initial droplet velocity	$\left|\overrightarrow{v_P}\right|$	$= 8.0\,m/s$
Droplet volume flow rate	$\dot{V}_P$	$= 33.9\,m^3/h$

Droplet diameter d_P was sampled from a Gaussian distribution with a mean diameter of $\bar{d}_P = 876.5\,\mu m$ and a standard deviation of $300\,\mu m$.

5.2. Droplet and air velocities

In order to compare numerical and experimental results simulations were performed for 4 different values of gas flow velocity at the inlet cross section $u_{F_{in}} = 1.0\,m/s;\ 2.0\,m/s; 3.0\,m/s$ and $4.0\,m/s$. Fig. 6 shows the calculated streamlines for the 4 different inlet gas velocities. A recirculating flow around the injection point of the droplets is formed due to phase interaction between the gas flow and the droplet spray with high droplet loading near the nozzle. The size of the domain of recirculating flow depends on the inlet gas velocity. Fig. 7 shows that most of the droplets are leaving the

flow domain through the inlet cross section of the gas flow at $x = 0.0$. For low inlet gas velocities only a small number of small droplets is affected by the recirculating flow and is carried by the gas flow to the upper outlet cross section. With increasing inlet gas velocity the number and the diameter of droplets reaching the domain above the injection point and the outlet cross section also increases. Due to lower gas velocities in this domain above the nozzle the larger droplets are moving towards the cylinder wall and are falling back along the wall (Fig. 7). In case of higher inlet gas velocities a second recirculating flow was observed near the wall of the test section above the injection point.

Fig. 8–11 show comparison of calculated gas and droplet velocities with measurements of Schulze et al. [12, 13] at 4 different cross sections of the cylindrical chamber at $x = 1.15\,m$; $1.55\,m$; $1.95\,m$ and $2.35\,m$. For the velocities of the particulate phase only 10% of the 2000 numerically predicted values are presented here. Also for the measured values of droplet velocities only the mean velocities are shown in the Fig. 8–11. The error bars were omitted in the diagrams because of the high information density. In the diagrams of Fig. 8–11 the gas and droplet velocities are normalized with the initial droplet velocity $\left|\overrightarrow{v_P}\right| = 8\,m/s$.

Diagrams show the downward recirculating gas flow with negative velocities near the symmetry axis and the positive gas velocities near the wall of the cylindrical chamber. Droplet velocities in Fig. 8–11 show the development of the downward directed jet from the nozzle with the spreading angle of 90°. Near the wall a smaller number of droplets are following the upward gas flow. Diagrams in Fig. 10 and 11 for $u_{F_{in}} = 3.0\,m/s$ and $u_{F_{in}} = 4.0\,m/s$ show, that the increasing number of upward moving droplets leads to a more significant gas–droplet interaction in the region near the cylinder wall. The agreement of calculated and measured gas velocities is reasonably good. Local differences between experimental and numerical results in the region near the symmetry axis are due to the relativ small number of calculated droplet trajectories in connection with the small size of the control volumes of the numerical grid in that region. This leads to a slight overprediction of the gas–droplet phase interaction due to momentum exchange in the immediate vicinity of the symmetry axis.

For the greater differences between measured and calculated droplet velocities there are two main reasons.

At first the numerical code does'nt consider the degradation of droplets by droplet–droplet and droplet–wall interaction. Therefore the droplet diameter distribution in numerical calculations is only determined by the initial droplet diameter distribution at the inlet cross section of the nozzle. Under real flow conditions various interaction processes produce a significant number of small droplets which are aible to follow the gas flow more closely. This small droplets are shifting the local droplet diameter distribution and the mean of the droplet velocity measurements.

Another reason for the differences in the predicted droplet velocities is the not so reliable measurement method used in the experiments of Schulze et al. [12]. As authers have mentioned in [13], it was impossible to use a phase–Doppler anemometer for concurrent measurements of the gas and droplet velocities. A laser–Doppler anemometer was used instead, which has measured velocities of droplets with a diameter $d_P \geq 30\,\mu m$. That leads to a dependence of the measured mean droplet velocity from the local droplet diameter distribution. These differences need further investigations related to the development of the droplet diameter distribution in the flow domain.

6. CONCLUSIONS

A numerical study of a gas–droplet flow was performed based on the Eulerian/Lagrangian approach taking into account the influence of gas–droplet interaction due to momentum exchange and the influence of fluid turbulence on the droplet motion. The comparison of the numerical simulations with experiments for a gas–droplet flow around a solid cone nozzle in a cylindrical chamber showed good agreement which indicates that the most important physical effects altering the gas flow and the droplet motion have been included in the calculation by the appropriate models.

References

[1] Crowe C.T., Sharma M.P., Stock D.E., 1977, "The Particle–Source–In Cell (PSI–Cell) Model for Gas–Droplet Flows," *Trans. of ASME, J. Fluids Eng.*, Vol. 99, pp. 325–332.

[2] Crowe C.T., 1982, "REVIEW — Numerical Models for dilute Gas–Particle Flows," *Trans. of ASME, J. Fluids Eng.*, Vol. 104, pp. 297–303.

[3] Durst F., Milojevic D., Schönung B., 1983, "Eulerian and Lagrangian Predictions of Particulate Two–Phase Flows — A Numerical Study," SFB 80/T/222, Preprint of the Sonderforschungsbereich 80, Ausbreitungs– und Transportvorgänge in Strömungen, University Karlsruhe, Germany.

[4] Milojević D., 1990, "Lagrangian Stochastic–Deterministic (LSD) Predictions of Particle Dispersion in Turbulence," *Part. Part. Syst. Charact.*, Vol. 7, pp. 181–190.

[5] Morsi S.A., Alexander A.J., 1972, "An Investigation of Particle Trajectories in Two–Phase Flow Systems," *J. Fluid Mech.*, Vol. 55, part 2, pp. 193–208.

[6] Ormancey A., Martinon J., 1984, "Prediction of Particle Dispersion in Turbulent Flow," *Phys. Chem. Hydrodynamics,* Vol. 5, pp. 229–244.

[7] Patankar S.V., 1980, *"Numerical Heat Transfer and Fluid Flow,"* McGraw–Hill, New York.

[8] Perić M., 1989, "A Finite Volume Multigrid Method for Calculating Turbulent Flows," *Proc. 7th Symposium on Turbulent Shear Flows,* Vol. 1, pp. 7.3.1.–7.3.6., Stanford University, USA.

[9] Perić M., Gosman A.D., 1989, "User Manual for the FASTEST Computer Package — Two–Dimensional Flows in Complex Geometries : Grid Generation, Flow Prediction and Graphical Representation of Results," Lehrstuhl für Strömungsmechanik, University Erlangen–Nürnberg, Germany.

[10] Schönung B., 1987, "Comparison of Different Dispersion Models for Particles in Lagrangian and Eulerian Prediction Codes," *In : Proceedings of the International Conference on Fluid Mechanics,* Peking, July 1.-4. 1987, Peking University Press, China.

[11] Schuh M.J., Schuler C.A., Humphrey J.A.C., 1989, "Numerical Calculation of Particle–Laden Gas Flows Past Tubes," *AIChE Journal,* Vol. 35, No. 3, pp. 466–480.

[12] Schulze R., Gruß J., 1993a, "Numerische und experimentelle Untersuchungen von räumlichen Zweiphasen–Strömungen (gasförmig/ flüssig)," Internal Research Report of the Department of Multiphase Flow, Technical University Chemnitz–Zwickau, Germany.

[13] Schulze R., Petrak D., Hädrich Th., Trommer G., 1993b, "Geschwindigkeitsmessungen in einem Sprühturm mit einem Halbleiterlaser Velocimeter," *Proc. 2. Fachtagung der GALA e.V. "Lasermethoden in der Strömungsmesstechnik,"* 14.–18. September 1993, PTB Braunschweig, Germany.
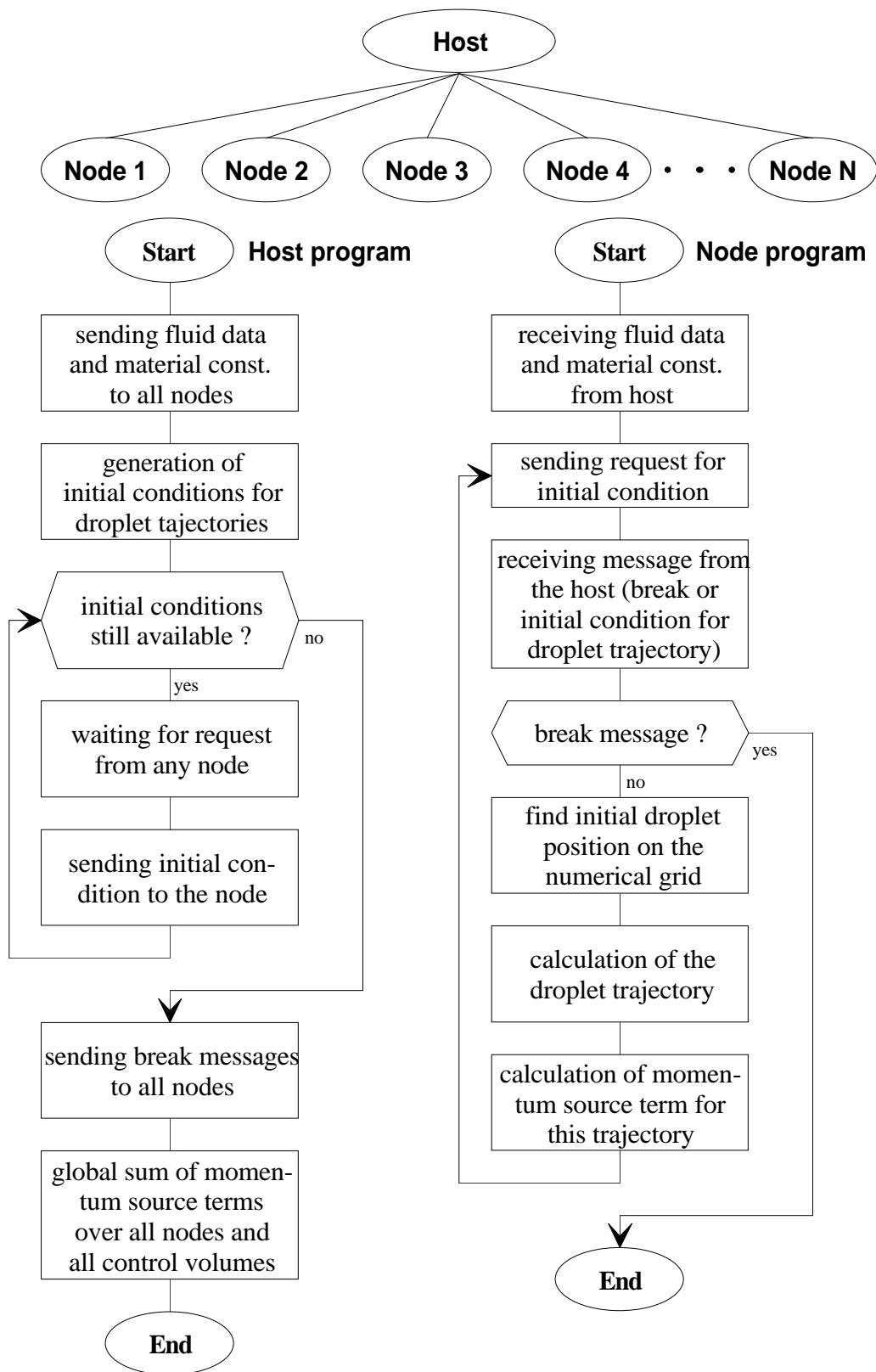
Figure 5: Flow chart of the host–node program structure of the Lagrangian solver.

This picture was to large to integrate it in this document !

Figure 6: Streamlines of gas–droplet flow.

This picture was to large to integrate it in this document !

Figure 7: Droplet trajectories for 2 different velocities at the inlet cross section $u_{F_{in}} = 1.0\,m/s$ and $u_{F_{in}} = 4.0\,m/s$.

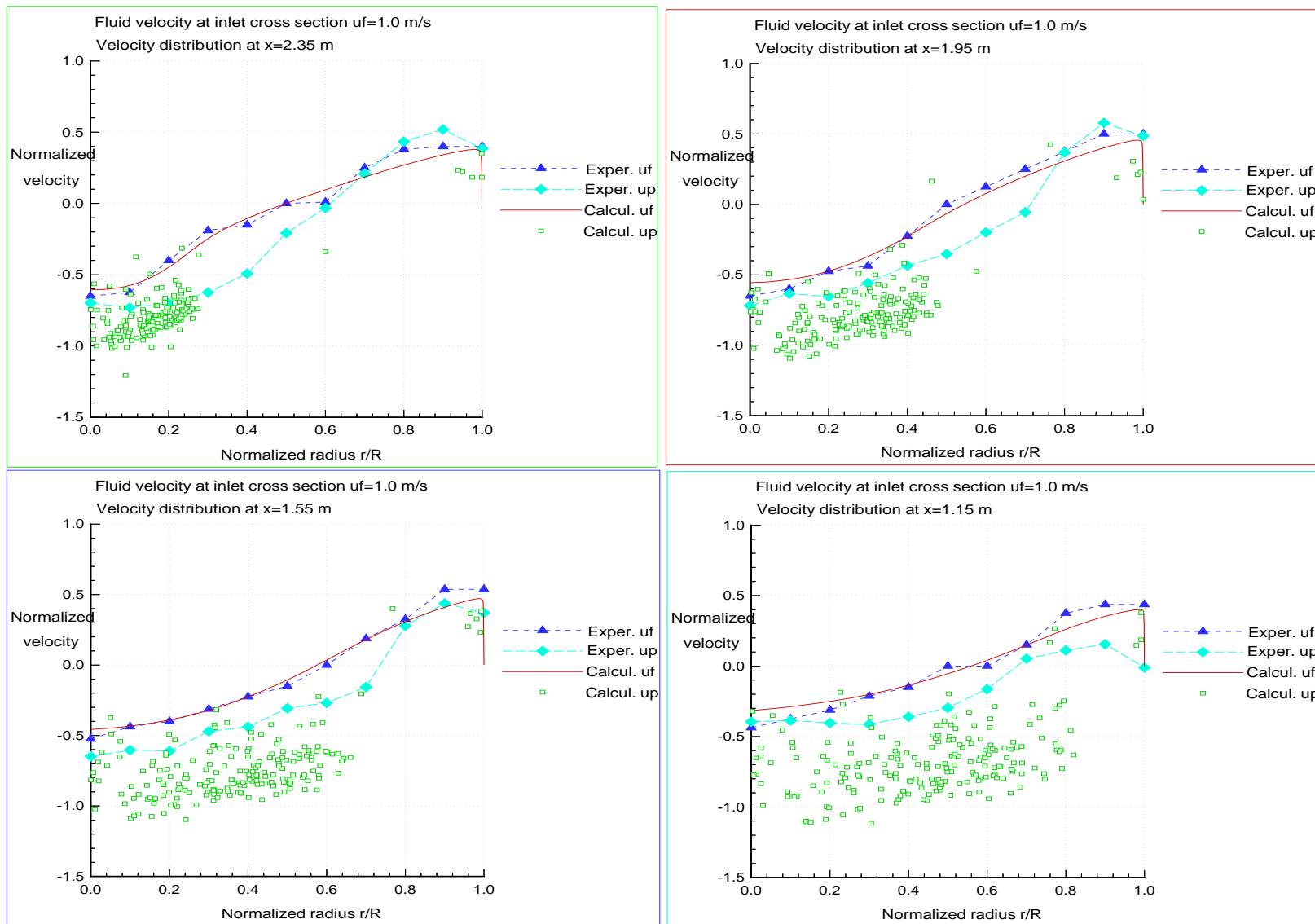Figure 8: Gas and droplet velocity distributions for $u_{F_{in}} = 1.0\,m/s$.

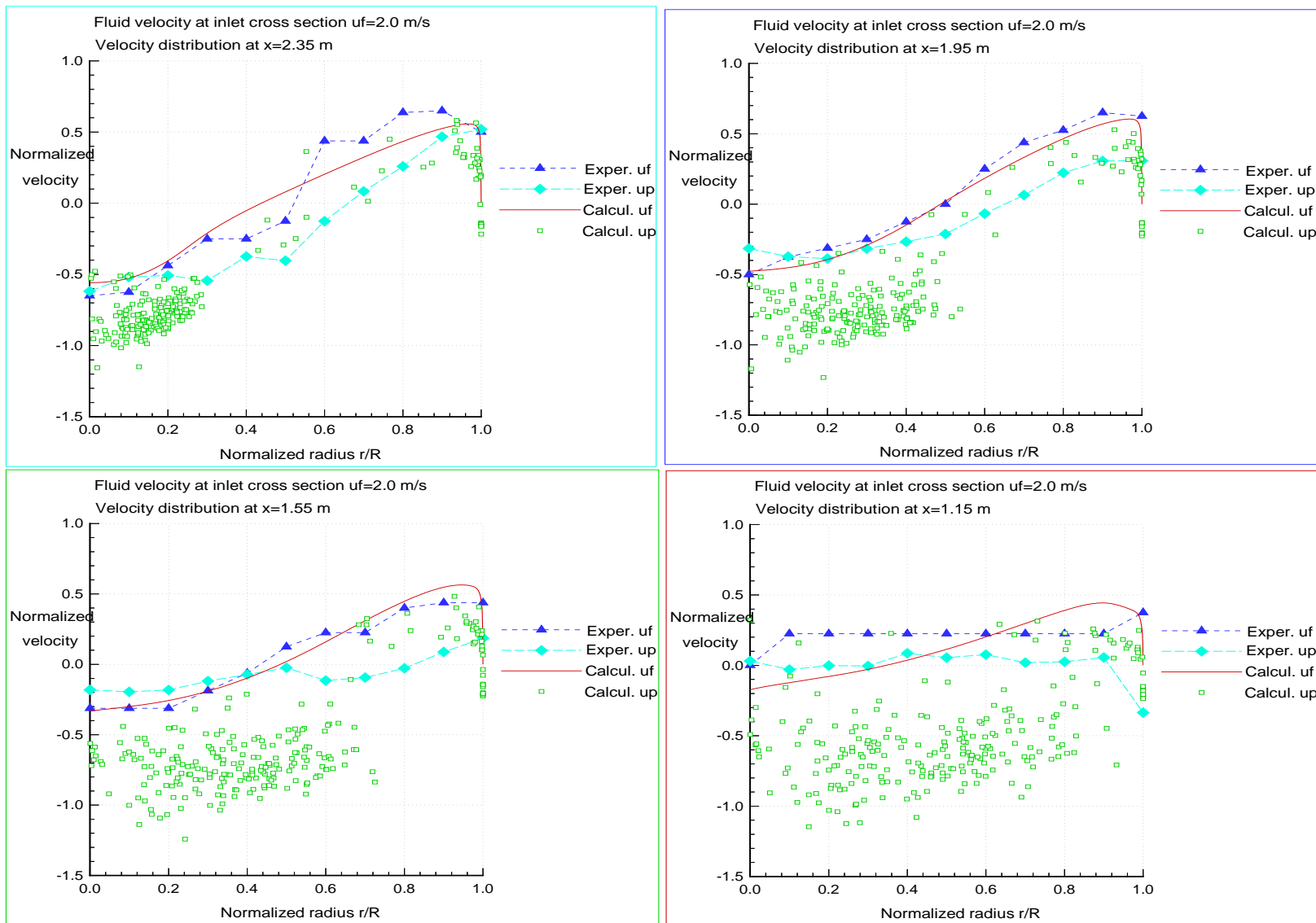Figure 9: Gas and droplet velocity distributions for $u_{F_{in}} = 2.0\,m/s$.

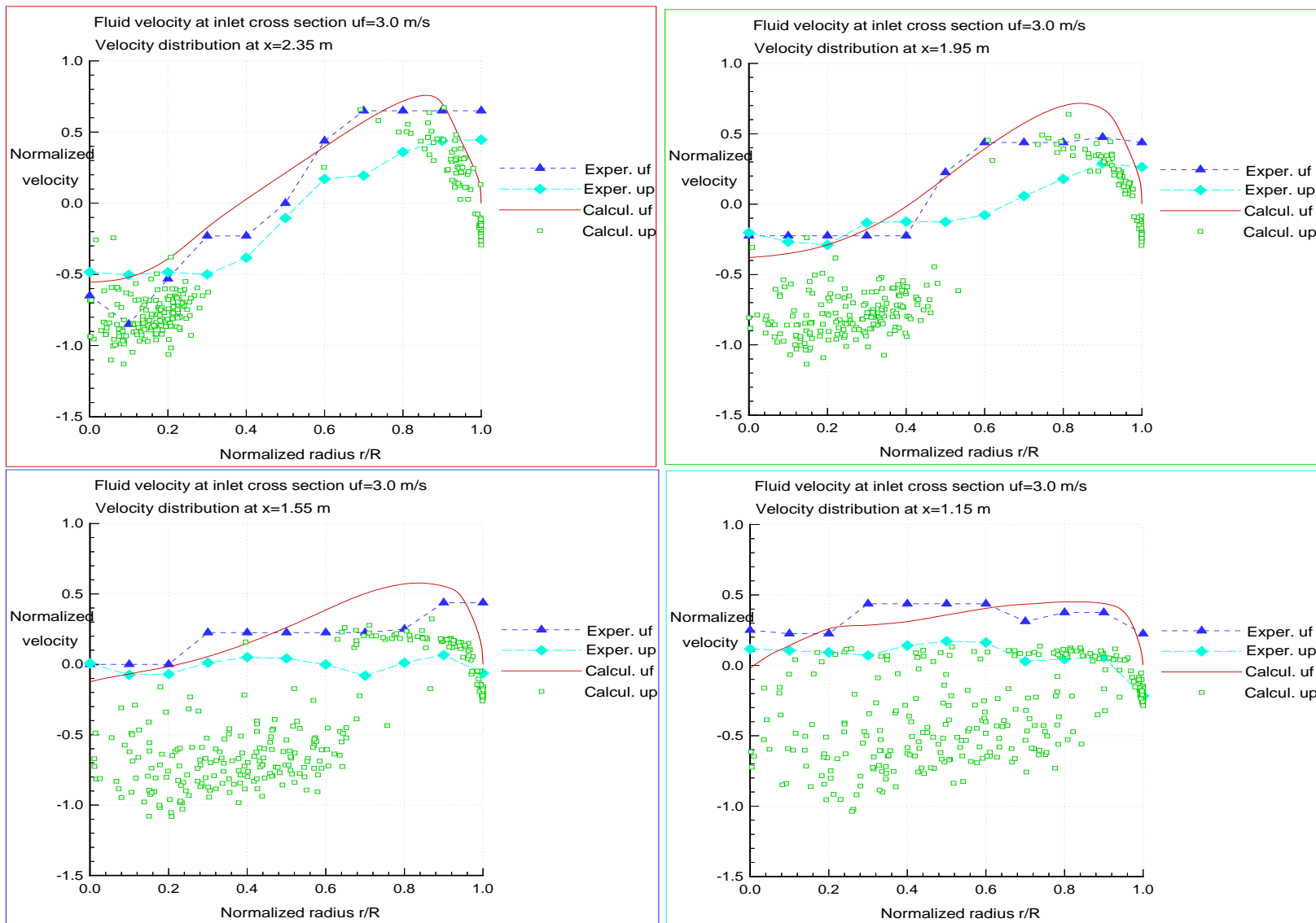Figure 10: Gas and droplet velocity distributions for $u_{Fin} = 3.0\,m/s$.

Figure 11: Gas and droplet velocity distributions for $u_{F_{in}} = 4.0\,m/s$.